The Influence of Stratification on the Inertial Recirculation

ZHENGYU LIU

Department of Atmospheric and Oceanic Sciences, University of Wisconsin—Madison, Madison, Wisconsin

(Manuscript received 29 April 1994, in final form 13 November 1996)

ABSTRACT

A two-layer quasigeostrophic model is used to investigate the influence of stratification on the inertial recirculation in a full basin model. It is found that the barotropic transport of the inertial recirculation is intensified significantly through barotropic–baroclinic interactions in the presence of a shallow thermocline or a strong stratification. Weakly nonlinear theories and numerical experiments show that a strong baroclinic–barotropic interaction intensifies the advection of potential vorticity anomaly toward the inertial recirculation and therefore forces a stronger recirculation. Furthermore, from the potential vorticity point of view, our model recirculations belong to the generalized ''modonlike'' recirculation (with $dQ/d\psi < 0$). The increased zonal penetration of recirculation cells with stratification is not caused by the internal dynamics of the recirculation cells. Instead, it is caused by the increased advection of potential vorticity anomaly—an external forcing to the recirculation cells.

1. Introduction

One striking feature of the North Atlantic circulation is the strong recirculation cells flanking the exit region of the Gulf Stream (Worthington 1976; Wunsch and Grant 1982; Schmitz 1980; Hogg 1983). Recent studies have shed light on the dynamics of the recirculation (Marshall and Nurser 1986; Greatbatch 1987; Ierley 1987; Cessi et al. 1987; Cessi 1988, C88 hereafter; Ierley and Young 1988). Barotropic processes have been found important for the establishment of the inertial recirculations. Observations show that the core of the recirculation cell is relatively depth-independent compared to the rest part (Schmitz 1980; Richardson 1985). Numerical experiments and theories in barotropic models also demonstrate that the barotropic process alone is able to establish a strong inertial recirculation (e.g., Bryan 1963; Cessi et al. 1987; Greatbatch 1988; Marshall and Marshall 1992, MM hereafter).

At the same time, it is also straightforward that the presence of stratification can significantly change the baroclinic structure of the recirculation. Strong stratification exists in the region of observed recirculations. This stratification tends to trap the wind-driven circulation in the thermocline, resulting in an intensified upper-layer recirculation (Holland and Rhines 1980; Marshall and Nurser 1986; Greatbatch 1987; C88). In addition, there is a strong local diabatic surface forcing in the region of the inertial recirculation. Recent theories have shown that this diabatic forcing is able to produce a substantial baroclinic recirculation in the upper ocean (Cushman-Roisin 1987; Huang 1990).

One natural question is then how the stratification affects the barotropic flow of the recirculation. In the interior ocean, the barotropic circulation is determined by the Sverdrup relation, which is independent of stratification (in the absence of topography). This is because the advection of relative vorticity is negligible, and therefore the barotropic flow is decoupled from the baroclinic flow. However, unlike in the interior ocean, relative vorticity is crucial in the recirculation and the western boundary layer. Thus, the barotropic flow is strongly coupled with the baroclinic flow. One may speculate that the stratification can significantly affect the barotropic circulation through the nonlinear interaction between the barotropic and baroclinic flows in the region of the recirculation and western boundary current. This will be confirmed in the paper. We will show that the inertial recirculation will be intensified substantially by either the structure or the intensity of the stratification through baroclinic–barotropic interactions.

Our study will emphasize the dynamic linkage between the recirculation and the western boundary current (WBC). In contrast, previous theories have focused on the local dynamics of the recirculation. A potential vorticity anomaly (Q anomaly) is prescribed as a boundary forcing to drive the recirculation. This Q anomaly, however, is determined by the matching of the recirculation with the basin-scale flow, and therefore cannot be studied in a regional model. In a regional model, C88 showed that the barotropic transport of a stratified re-

Corresponding author address: Zhengyu Liu, Department of Atmospheric and Oceanic Sciences, University of Wisconsin—Madison, Madison, WI 53706-1695.
E-mail; znl@ocean.meteor.wisc.edu

circulation is determined mainly by the barotropic Q anomaly on the boundary of a recirculation cell. Thus, the recirculation would remain unchanged if the barotropic Q anomaly remains unchanged. However, in a full basin study, an altered stratification may strongly affect the WBC and its advection of Q anomaly. Thus, stratification may change the barotropic transport of the recirculation significantly.

This paper will be arranged as follows. Section 2 presents the numerical results, focusing on the effect of the structure and intensity of the stratification on the recirculation. The stratification effect is first studied in terms of vorticity dynamics with a weakly nonlinear theory in section 3 and with numerical experiments in section 4. Then, the stratification effect is examined in terms of potential vorticity (Q) distribution. A summary and additional discussions are given in section 6.

2. Numerical experiments

a. Model and experiments

We will use the two-layer quasigeostrophic (QG) model whose upper layer and lower layer simulate the thermocline and abyssal water respectively. The following nondimensional equations will be used throughout the paper:

$$\partial_t q_1 + J(\psi_1, q_1) = w_e/h_1 + d\nabla^2 q_1 \qquad (2.1a)$$

$$\partial_t q_2 + J(\psi_2, q_2) = d\nabla^2 q_2, \qquad (2.1b)$$

where the upper- and lower-layer nondimensional Q are, respectively,

$$q_1 = a[\nabla^2\psi_1 + f_1(\psi_2 - \psi_1)] + y \qquad (2.1c)$$

$$q_2 = a[\nabla^2\psi_2 + f_2(\psi_1 - \psi_2)] + y. \qquad (2.1d)$$

Here, with standard notations, and denoting the corresponding dimensional quantities with a star, the nondimensional quantities are defined as

$$(x, y) = \frac{(x^*, y^*)}{L}, \quad t = \frac{t^*}{T}, \quad (\psi_1, \psi_2) = \frac{(\psi_1^*, \psi_2^*)}{\Psi},$$

$$w_e = \frac{w_e^*}{W_0}, \quad (h_1, h_2) = \frac{(H_1, H_2)}{H}$$

$$\Psi = \frac{f_0 W_0 L}{\beta H}, \quad T = \frac{L^2}{\Psi}, \quad a = \frac{\Psi}{\beta L^3},$$

$$f_n = \frac{L^2 f_0^2}{g' h_n^*}, \quad d = \frac{d^*}{\Psi}, \qquad (2.2)$$

where the dimensional quantities are chosen as the horizontal length scale $L = 2000$ km; the total depth $H = 4$ km; the magnitude of Ekman pumping $W_0 = 10^{-4}$ cm s^{-1}; the lateral viscosity $d = 1.4 \times 10^6$ cm^2 s^{-1}; the Coriolis parameter $f_0 = 10^{-4}$ s^{-1}; and $\beta = 1.3 \times 10^{-13}$ cm^{-1} s^{-1}. This gives the barotropic Sverdrup velocity on the order of $\Psi/L = 0.2$ cm s^{-1} and the corresponding advective timescale $T = 30$ yr. Two parameters that determine the stratification will be varied in our experiments: the reduced gravity g', which determines the intensity of the stratification, and the thermocline depth H_1 (or the lower-layer thickness $H_2 = H - H_1$), which determines the structure of the stratification.

The equations are solved with a leapfrog time stepping and a free-slip lateral boundary condition. Streamfunctions are derived from potential vorticities by a FFT elliptical solver. A rectangular basin $(0, 0.5L) \times (-0.5L, 0.5L)$ is adopted with a horizontal resolution of 16 km in both longitude and latitude. The Ekman pumping adopts the form $w_e(y) = \sin[2\pi(y - y_0)]$, where the intergyre boundary is located at $y_0 = 0.05$. In the following, we will only discuss the subtropical gyre unless otherwise specified.

The control run uses a standard stratification that resembles observations: $g' = 2$ cm s^{-2} and $H_1 = 1$ km, $H_2 = 3$ km. The streamfunctions for the final steady circulations are presented in Figs. 1a–d for the upper-layer, lower-layer, barotropic ($\psi_B = h_1\psi_1 + h_2\psi_2$), and baroclinic ($\psi_C = \psi_1 - \psi_2$) flows respectively. The most important feature is a pair of recirculation cells flanking the exit region of the midlatitude jet. The recirculation cell is strong in the upper-layer, barotropic, and baroclinic flow fields, but weak in the lower layer. Upper- and lower-layer Q are presented in Fig. 1e and Fig. 1f, respectively. The upper-layer Q is characterized by a strong front along the intergyre boundary and a relatively uniform Q pool within the recirculations. The lower layer is characterized by a single homogenized Q pool containing both recirculation cells. The nondimensional maximum Sverdrup transport now is $\psi_B = 0.5$ [corresponding to 8 Sv (Sv $\equiv 10^6$ m^3 s^{-1})]. However, the maximum barotropic flow in the control run reaches a maximum of about $\psi_B = 1.2$, which is more than twice the interior Sverdrup transport.

We will discuss the final equilibrium state of two sets of experiments, each with five experiments (Table 1). The first set (DPs) is designed to test the effect of the vertical structure of stratification on the recirculation, with the thermocline depth h_1 different in the experiments (the total depth is fixed); the second set (RGs) tests the effect of the intensity of the stratification on the recirculation, with the value of the reduced gravity changing in each experiment.

b. Effect of thermocline structure

The effect of the vertical thermocline structure on recirculation can be seen in the barotropic flow of the five experiments in Fig. 2. These experiments have the same total depth, but different upper-layer thickness, or thermocline depth. The control run is replotted here as DP_0 in Fig. 2b. The thermocline depth is increased to 2 km in run DP_{-1} (Fig. 2c). The interior flow remains unchanged, as determined from the Sverdrup relation. However, the inertial recirculation is weakened sub-

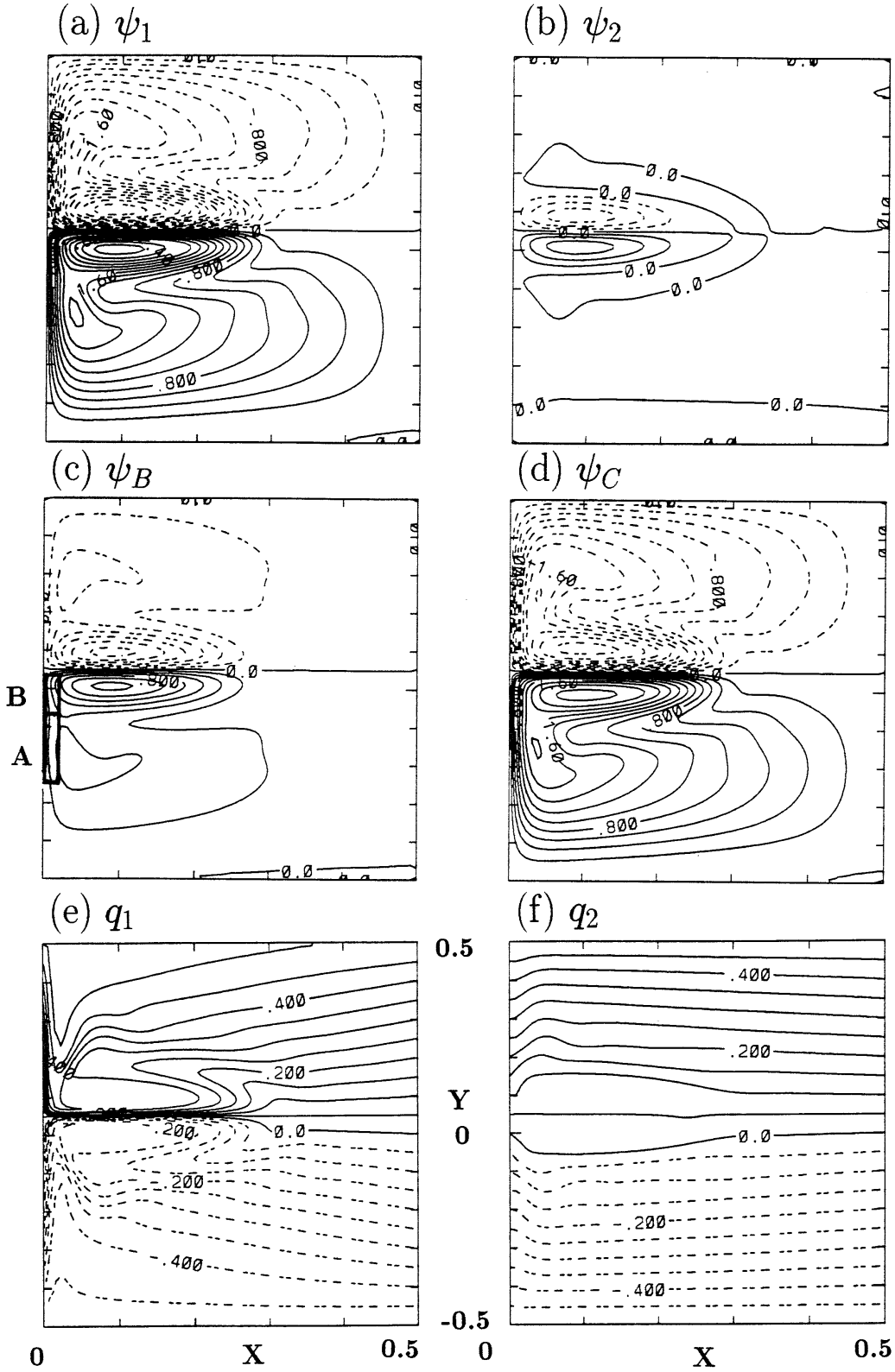

FIG. 1. The flow and potential vorticity field for the control run. Nondimensional streamfunctions are shown for (a) upper-layer, (b) lower-layer, (c) barotropic, and (d) baroclinic flows. The contour interval is 0.2. Nondimensional potential vorticity is shown for (e) upper-layer and (f) lower-layer flows. The contour interval is 0.05. In (c), the region A and region B are for vorticity term balances in Fig. 5.

TABLE 1. Table for experiments. For DPs $g' = 2$ cm s^{-2}; for RGs $H_1 = 1$ km.

	DP_{-3}	DP_{-2}	DP_{-1}	DP_0	DP_{+1}
H_1 (km)	4	3	2	1	0.5
	RG_{-3}	RG_{-2}	RG_{-1}	RG_0	RG_{+1}
g' (sm s^{-2})	0.02	0.2	1	2	4

stantially in both its strength and size. A further increase of thermocline depth results in a further weakening of the recirculation, as shown in DP_{-2} (Fig. 2d) and DP_{-3} (Fig. 2e, which is identical to the barotropic case because of a zero lower-layer thickness). In contrast, if the thermocline depth is reduced by a half from that of the control run, the recirculation is intensified substantially as seen in DP_{+1} of Fig. 2a. This set of experiments suggests that, unlike in the interior ocean, the barotropic flow of the recirculation can be affected substantially by the structure of the stratification: the recirculation intensifies with a shallower thermocline depth.

c. *Effect of stratification intensity*

The effect of stratification intensity on recirculation can be seen in the barotropic flows of the five experiments in Fig. 3. These experiments have the same thickness for the upper and lower layer, but different interfacial reduced gravity. The control run is again shown in Fig. 3b for reference (RG_0). With the reduced gravity decreased by a half in RG_{-1} (Fig. 3c), the recirculation weakens substantially, while the interior flow remains unchanged. A further reduction of the reduced gravity in RG_{-2} (Fig. 3d) leads to a further weakening of the recirculation. Figure 2d resembles closely the pure barotropic flow (see Fig. 2e) because of the extremely weak stratification. A further reduction of the reduced gravity by a order in RG_{-3} (not shown) only produces a slight reduction of the recirculation. In contrast, if the reduced gravity is doubled that of the control run as in RG_{+1} (Fig. 3a), the recirculation is intensified significantly. Thus, the recirculation intensifies with an increased stratification. The recirculation is particularly sensitive to the reduced gravity near the observed values.

The rest of the paper intends to understand the physical mechanism through which stratification affects the recirculation. As an introduction, we first notice one common feature in both sets of experiments: the barotropic flow of the inertial recirculation increases (decreases) with the strength of the upper (lower)- layer flow or the baroclinic flow. A shallower thermocline depth tends to increase the upper-layer flow, but to decrease the lower-layer flow. This in turn results in an intensified baroclinic flow. In the interior ocean where relative vorticity is negligible, the change in the baroclinic flow is unable to feed back on the barotropic flow field, which is governed by the Sverdrup relation. However, in the western boundary layer/recirculation region where relative vorticity is crucial, the barotropic and baroclinic flow are strongly coupled. It is therefore conceivable that a change in the baroclinic flow can feed back on the barotropic flow through baroclinic–barotropic interactions. (The effect of the reduced gravity is more subtle. It involves dissipation processes in the boundary layer as will be seen soon.) C88 has pointed out that the barotropic transport of recirculation is mainly determined by the barotropic Q anomaly injected by the midlatitude jet. Since the Q anomaly is advected by the WBC toward the midlatitude jet, one may further speculate that the change of the recirculation under various stratification may be affected strongly by the altered WBC due to barotropic–baroclinic interactions. This speculation is confirmed in the following two sections.

3. A weakly nonlinear theory: The vorticity dynamics

We first present a weakly nonlinear analysis to show the effect of stratification on the WBC. Rewriting the steady form of (2.1a,b) in terms of the barotropic and baroclinic streamfunctions, we have

$$[-d\nabla^4 + \partial_x]\psi_B = w_e - aJ(\psi_B, \nabla^2\psi_B) - ah_eJ(\psi_C, \nabla^2\psi_C) \tag{3.1a}$$

$$\left\{-d\left[\nabla^2 - \left(\frac{L}{L_D}\right)^2\right]\nabla^2 + \partial_x\right\}\psi_C = \frac{w_e}{h_1} - aJ\left\{\psi_B, \left[\nabla^2 - \left(\frac{L}{L_D}\right)^2\right]\psi_C\right\} - aJ\{\psi_C, \nabla^2[\psi_B + (h_2^2 - h_1^2)\psi_C]\}, \tag{3.1b}$$

where $h_e = h_1h_2$ is the equivalent depth and $L_D = \sqrt{g'H_1H_2/H}/f_0$ is the deformation radius. In the interior ocean, relative vorticity is negligible. The barotropic and baroclinic flows are determined by

$$\partial_x\psi_{BI} = w_e \tag{3.2a}$$

$$\partial_x\psi_{CI} = w_e/h_1. \tag{3.2b}$$

This is a Sverdrup flow in the upper layer and no motion in the lower abyssal layer: $\partial_x\psi_{1I} = w_e/h_1$, $\partial_x\psi_{2I} = 0$.

The dynamics in the western boundary layer are much more complicated. In order to show explicitly the role of

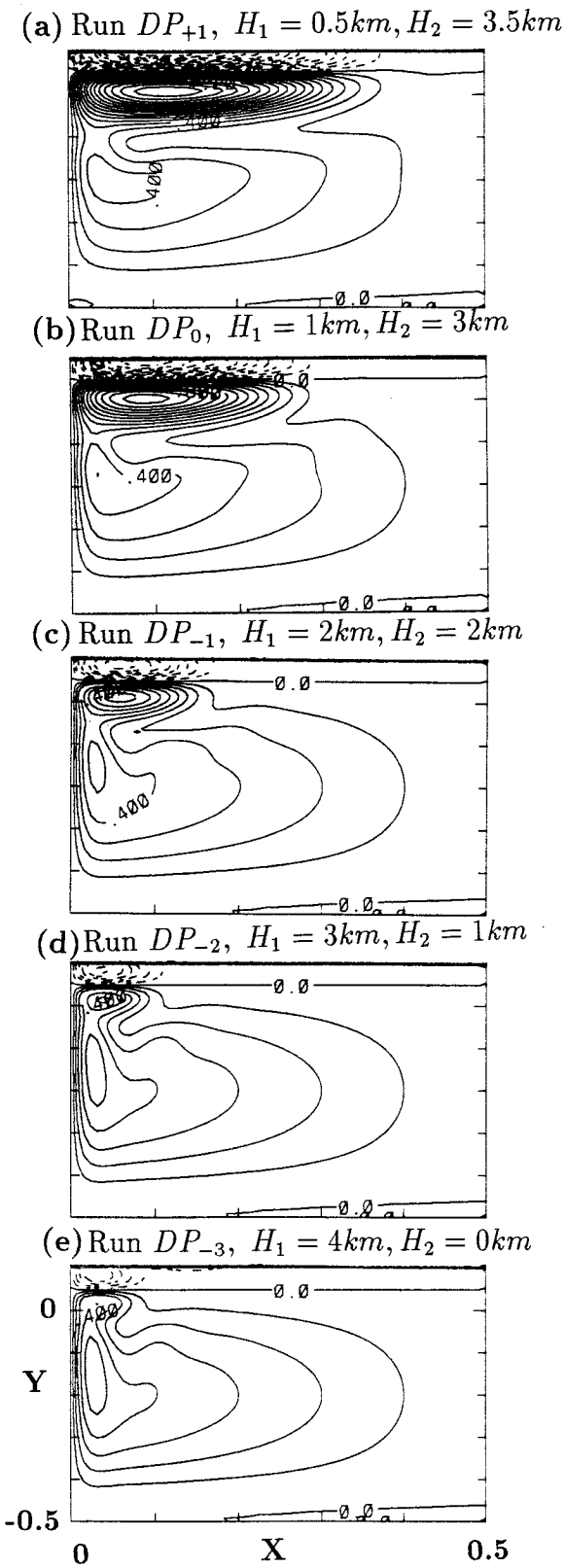

FIG. 2. The nondimensional barotropic streamfunction for the five runs with different thermocline depths (DP). The dimensional total depth is H = 4 km for all the runs, but the upper-layer depth decreases as (a) H_1 = 0.5 km, (b) H_1 = 1 km, (c) H_1 = 2 km, (d) H_1 = 3 km, and (e) H_1 = 4 km. The contour interval is 0.1. While the interior flow remains unchanged, the recirculation is intensified dramatically with a shallower thermocline depth. In the figure, most of the subpolar gyre is not shown.

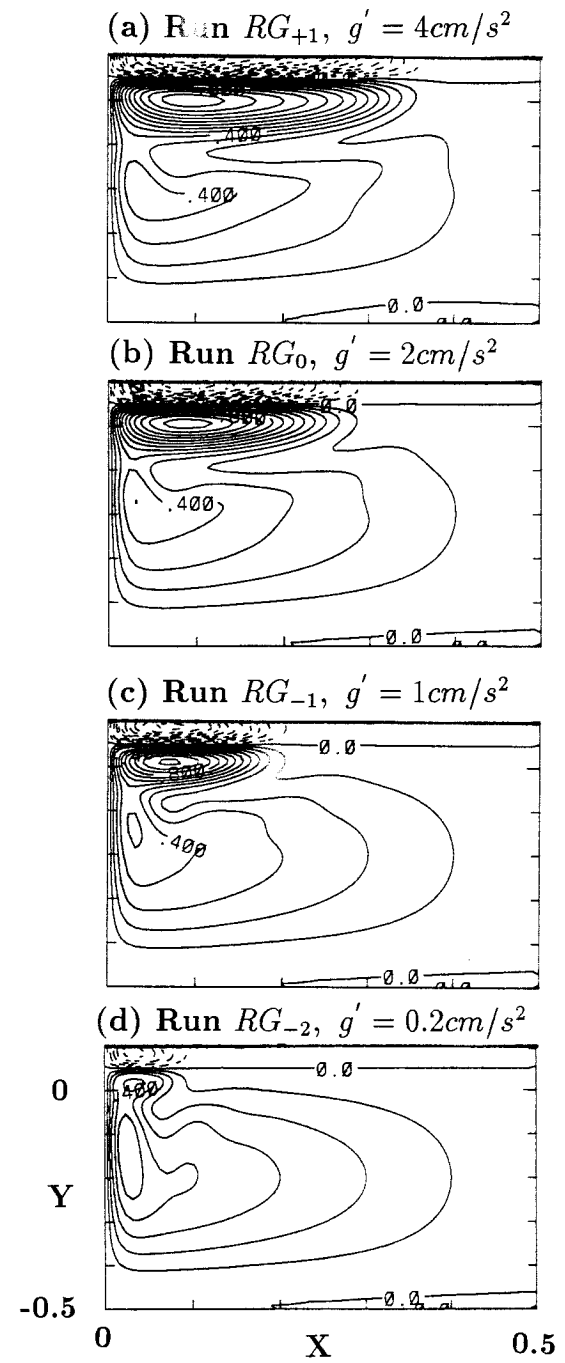

FIG. 3. Similar to Fig. 2 but for four runs with different reduced gravity (RG): (a) g' = 4 cm s^{-2}, (b) g' = 2 cm s^{-2}, (c) g' = 1 cm s^{-2}, and (d) g' = 0.2 cm s^{-2}. While the interior flow remains unchanged, the recirculation is intensified dramatically for a larger reduced gravity. The recirculation is particularly sensitive to the reduced gravity at the order of observed values.

barotropic–baroclinic interaction, we derive the boundary layer equations. We first denote $\delta_M = (d^*/\beta)^{1/3}$ and $\delta_I = [\Psi/(L\beta)]^{1/2}$ as widths of the Munk boundary layer and the inertial boundary layer respectively (Pedlosky 1987). In terms of the boundary layer variable $\xi = xL/\delta_M$, the boundary layer equations can be derived from (3.1) as

$$[-\partial_{\xi\xi\xi} + 1]\partial_\xi \psi_B = -\epsilon\{J(\psi_B, \partial_{\xi\xi}\psi_B) + h_e J(\psi_C, \partial_{\xi\xi}\psi_C)\} \tag{3.3a}$$

$$[-(\partial_{\xi\xi} - b)\partial_\xi + 1]\partial_\xi \psi_C = -\epsilon\{J[\psi_B, (\partial_{\xi\xi} - b)\psi_C] - J[\psi_C, \partial_{\xi\xi}(\psi_B + (h_2^2 - h_1^2)\psi_C)]\}, \tag{3.3b}$$

where the nondimensional parameters are $\epsilon \equiv (\delta_I/\delta_M)^2$ and $b \equiv (\delta_M/L_D)^2 \sim 1/g'$, representing the nonlinearity and stratification intensity respectively. We will discuss the weakly nonlinear limit $\epsilon \ll 1$ in this section.

a. A preliminary analysis

First, a crude analysis will be helpful for the understanding of the role of stratification and the mechanism of barotropic–baroclinic interaction. The barotropic vorticity equation (3.3a) has two nonlinear terms: the barotropic–barotropic interaction term $-J(\psi_B, \partial_{\xi\xi}\psi_B)$ and the baroclinic–baroclinic interaction term $-h_e J(\psi_C, \partial_{\xi\xi}\psi_C)$. They represent the advection by the barotropic flow of barotropic relative vorticity and the advection by the baroclinic flow of baroclinic relative vorticity, respectively. Both terms can contribute to the barotropic flow. However, the stratification affects the barotropic flow mainly through the baroclinic–baroclinic interaction, because the barotropic–barotropic interaction is independent of stratification at the first order as in (3.2a). In addition, the interior baroclinic flow increases for a shallower thermocline depth because of the factor $1/h_1$ in Eq. (3.2b). Thus, the increase in the barotropic transport due to the net effect of the baroclinic–baroclinic interaction, denoted by $\Delta\psi_B \mid_C$, varies with h_1 as

$$\Delta\psi_B \mid_C \sim \epsilon h_e \psi_C^2 \sim \epsilon w_e^2 h_2/h_1, \tag{3.4}$$

where the transport of the WBC is assumed to be of the same order as the interior flow $\psi_C \sim \psi_{CI}$. Equation (3.4) shows clearly that a shallower h_1 can affect the barotropic transport in the western boundary layer dramatically.

The role of the reduced gravity can be further seen in the limit of a weak stratification $b \to \infty$. Neglecting a free-slip sublayer, Eq. (3.3b) for the baroclinic flow can be approximated at the lowest order as

$$(b\partial_\xi + 1)\partial_\xi \psi_C = 0. \tag{3.5}$$

The boundary layer solution is

$$\psi_{C0} = \psi_{CI}(1 - e^{-\xi/b}). \tag{3.6}$$

A larger b gives a wider width of the boundary layer $l_b \sim b$. From Eq. (3.3a), one then obtains

$$\Delta\psi_B \mid_C \sim \epsilon h_e \psi_C^2/l_b^2 \sim \epsilon w_e^2 h_2/(h_1 b^2). \tag{3.7}$$

Thus, an increase in stratification (smaller b) leads to an enhancement of baroclinic–baroclinic interaction on WBC. This occurs because a stronger stratification gives a larger deformation radius and therefore reduces the stretching component of potential vorticity, which would result in a reduction of vorticity diffusion toward the interior ocean if the boundary layer thickness remains unchanged. To balance the total vorticity input over the basin, a narrower boundary layer is therefore needed that enhances the Q diffusion. This narrower boundary layer enhances the relative vorticity and in turn the advected Q anomaly.

It should be noticed that the crude analysis here does not address the other important issue: the sign of the nonlinear advection term. This will be discussed in the formal analysis below.

b. Weakly nonlinear analysis

Now we discuss the general weakly nonlinear cases. The streamfunctions in the boundary layer will be expanded as

$$\psi_B = \psi_{B0} + \epsilon\psi_{B1} + O(\epsilon^2),$$
$$\psi_C = \psi_{C0} + \epsilon\psi_{C1} + O(\epsilon^2). \tag{3.8}$$

The lowest order solutions ψ_{B0} and ψ_{C0} are the linear Munk-type solution [appendix A and B, Eqs. (A.3) and (B.4)]. The next order barotropic solution ψ_{B1} is caused by the feedback of nonlinear interactions on the barotropic flow. The ψ_{B1} has two parts: $\psi_{B1} = \psi_{B1}^B + \psi_{B1}^C$, where ψ_{B1}^B and ψ_{B1}^C are caused respectively by the barotropic–barotropic interaction term and the baroclinic–baroclinic interaction term in Eq. (3.3a). A detailed derivation of the solution is given in appendix A and B. For our purpose, we only present the perturbation velocity of WBC corresponding to ψ_{B1}^B and ψ_{B1}^C. That is, $v_{B1} = v_{B1}^B + v_{B1}^C$, where

$$v_{B1}^B = \partial_\xi \psi_{B1}^B(\xi = 0) = -5\partial_y(\psi_{BI}^2)/12 \sim -\partial_y[w_e^2(y)] \tag{3.9a}$$

$$v_{B1}^C = \partial_\xi \psi_{B1}^C(\xi = 0) = -h_e \partial_y(\psi_{CI}^2)G(b) \sim -\partial_y[w_e^2(y)]h_2/h_1 G(b). \tag{3.9b}$$

In (3.9a,b), the interior flow ψ_{BI} and ψ_{CI} are given in (3.2a,b). The effect of reduced gravity (in b) appears only in the function $G(b)$, which is given in (B.8) and plotted in Fig. B1a.

c. Barotropic–barotropic interaction: Latitude shift of maximum WBC

We first discuss the effect of barotropic–barotropic interaction. The solution (3.9a) states that the WBC is accelerated in the northern half [$v^B_{B1} \sim -\partial_y(\psi^2_{BI}) > 0$] but is decelerated in the southern half [$v^B_{B1} - \partial_y(\psi^2_{BI}) < 0$] by barotropic–barotropic interaction. The separation latitude between the northern and the southern regions is located at $\partial_y(\psi^2_{BI}) = 0$, which is determined by the interior Ekman pumping for the linear basic state here. Thus, the maximum WBC is shifted north toward the intergyre boundary. Physically, since less (more) anticyclonic relative vorticity is advected northward in the southern (northern) half of the WBC, the required diffusive vorticity flux toward the interior ocean is reduced (enhanced). The reduced (enhanced) vorticity diffusion is then balanced by a weaker (stronger) planetary vorticity advection in the southern (northern) part of the WBC, implying a weaker (stronger) WBC there. This physical explanation is valid only in the weakly nonlinear case.

The shift of the maximum WBC should further induce changes of the recirculation. Since the inertial recirculation is established by the Q anomaly that is advected through the WBC, a stronger WBC converging toward the intergyre boundary should enhance the eastward penetration of the Q anomaly along the midlatitude jet. This establishes a stronger recirculation with a greater zonal penetration and meridional width (e.g., Cessi et al. 1987; Ierley and Young 1988). This explains, from a weakly nonlinear point of view, the dynamic linkage between the WBC and the recirculation.

d. Baroclinic–baroclinic interaction: The intensification

The effect of baroclinic–baroclinic interaction is similar to that of the barotropic–barotropic interaction. Since $G(b)$ is positive (Fig. B1a), v^C_{B1} has the same sign as v^B_{B1}. Thus, by reinforcing the barotropic–barotropic interaction, the baroclinic–baroclinic interaction enhances the shift of the WBC toward the midlatitude and therefore intensifies the recirculation.

Unlike the barotropic–barotropic interaction, however, the baroclinic–baroclinic interaction depends strongly on the stratification. The baroclinic–baroclinic interaction is proportional to $1/h_1$ [see (3.9b)] and b. [The dependence on b can be seen in Fig. B1a, which shows a monotonical decrease of $G(b)$ with b.] Thus, the baroclinic–baroclinic interaction intensifies in the presence of either a shallower thermocline or a larger reduced gravity (smaller b). The baroclinic–baroclinic interaction is particularly sensitive to the reduced gravity at the order of observed values. This can be seen in Fig. B1a, where the slope of the $G(b)$ function is greatest for $0(b) < 1$, which is close to observed values (the control run has $b = 1/3$). The intensification occurs because the surface Ekman pumping forcing is trapped more in the thermocline, which results in a stronger baroclinic circulation. The baroclinic flow then feeds back nonlinearly on the barotropic flow. In the opposite limit, with either $h_2 = 0$ or a zero reduced gravity [$b = \infty$, noticing $G(\infty) = 0$ in Fig. B1a], the effect of the baroclinic–baroclinic interaction vanishes.

In short, the weakly nonlinear theory seems to be able to explain qualitatively our numerical experiments for different thermocline depth (Fig. 2) and stratification intensity (Fig. 3). The stratification can strongly affect the recirculation through the baroclinic–baroclinic interaction, which feeds back on the barotropic flow of the WBC to increase the advection of Q anomaly and, in turn, enhances the recirculation.

4. Numerical analysis. I: Vorticity dynamics

Here we further analyze the vorticity dynamics of the numerical experiments to compare with our weakly nonlinear theory. We will only discuss the set of runs with different thermocline depth (DPs) because the other set (RGs) is similar (not shown).

a. Recirculation and Q anomaly

As the depth of thermocline decreases (from DP_{-3} to DP_{+1}), Fig. 4a shows a monotonic increase in the maximum barotropic transport, the zonal penetration distance, and the meridional width of the recirculation. The intensification of the recirculation is accompanied by an increase in the barotropic Q anomaly along the northern boundary of the subtropical gyre (Fig. 4b), consistent with previous theories (C88; Ierley and Young 1988). However, it is interesting to notice in Fig. 4b that the maximum Q anomaly, which occurs along the western boundary, remains almost unchanged for different experiments. Thus, it is the different zonal penetration of the Q anomaly that results in the different recirculation.

Furthermore, the increase of Q anomaly from run DP_{-3} to DP_{+1} (Fig. 4b) is accompanied by an increase (decrease) of boundary current speed in the northern (southern) part of the WBC. This is clear if one compares Fig. 4b with Fig. 5a, the latter of which plots the downstream profile of the WBC speed for each run.[1]

[1] The separation latitude between the northern acceleration part and the southern deceleration part of the WBC is located north of the middle of the subtropical gyre. This occurs because the basic state in the numerical experiment is not linear, and therefore the maximum

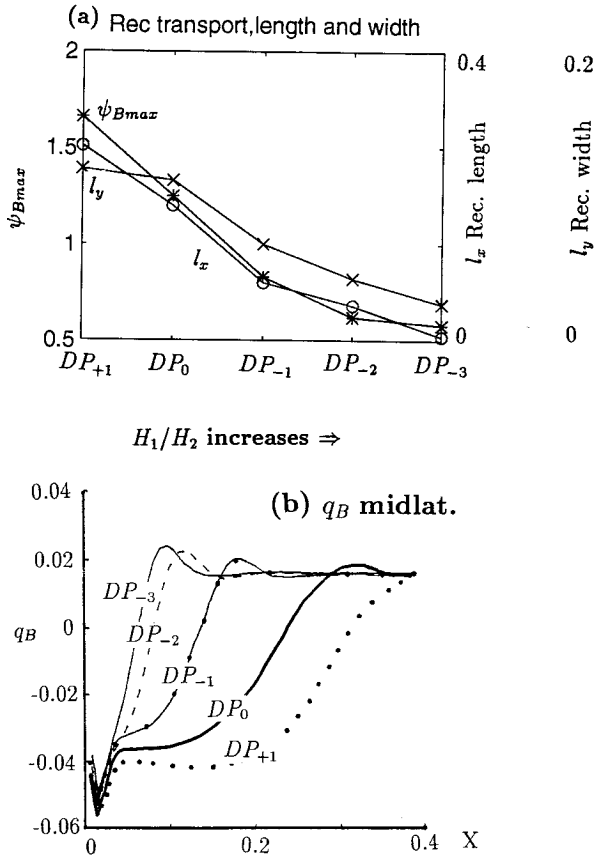

FIG. 4. (a) The maximum barotropic streamfunctions of the five DP experiments (star). The zonal penetration distance (circle) and meridional width (cross) of the barotropic recirculation are also plotted. The recirculation intensifies with a shallower thermocline depth. (b) Zonal penetration of the barotropic potential vorticity $q_B = h_1q_1 + h_2q_2$ averaged along the midlatitude jet on the subtropical side ($y = 0.008$ to $y = 0.031$) for the DP runs. The penetration of the potential vorticity anomaly increases for shallower thermocline depth.

This seems to be consistent with our weakly nonlinear theory. However, later discussions show that in strongly nonlinear experiments, this is not so.

b. Vorticity dynamics in the southern part of WBC

The vorticity balance in the southern deceleration part of the WBC is shown in Fig. 5b, which plots each term of the barotropic equation (3.3a) in the southern region. First, the local wind term is always negligible (not shown). The vorticity balance at the first order is between the planetary vorticity advection and dissipation (Munk type),

$$\partial_x\psi_B \sim \nabla^4\psi_B. \tag{4.1}$$

As h_1 decreases (from DP_{-3} to DP_{+1}), the total nonlinear advection (roughly the difference between $\partial_x\psi_B$ and $\nabla^4\psi_B$ curves) increases significantly and is accompanied by a strong reduction of the dissipation term. The planetary vorticity advection also exhibits a moderate reduction, which is consistent with the deceleration of WBC in this region (Fig. 5a). Furthermore, Fig. 5b shows that the increase of the nonlinear term is due to the rapid increase of the baroclinic–baroclinic interaction. In contrast, the barotropic–barotropic interaction decreases because of the reduction in barotropic current. Thus, for a reduced h_1 (or an increased $1/h_1$), the change of the vorticity equation is dominated by

$$\frac{\partial[-\nabla^4\psi_B]}{\partial(1/h_1)} \sim \frac{\partial[-h_eJ(\psi_C, \nabla^2\psi_C)]}{\partial(1/h_1)} > 0. \tag{4.2}$$

The perturbed planetary vorticity advection is then derived from (4.1) as

$$\frac{\partial(\partial_x\psi_B)}{\partial(1/h_1)} \sim \frac{\partial(\nabla^4\psi_B)}{\partial(1/h_1)} < 0. \tag{4.3}$$

This results in the reduction of the WBC speed. The results here agree with the weakly nonlinear study in section 3 and appendixes A and B.

c. Vorticity dynamics in the northern part of WBC

The vorticity balance becomes more complex farther north, as shown in Fig. 5c. In the cases of deep h_1 such as DP_{-3} and DP_{-2}, nonlinearity is weak and the vorticity balance is similar to (4.1)–(4.3), except for an opposite sign in the nonlinear advection

$$\frac{\partial[-h_eJ(\psi_C, \nabla^2\psi_C)]}{\partial(1/h_1)} < 0.$$

This advection implies a northward advection of more anticyclonic relative vorticity, and therefore accelerates the WBC as discussed in the weakly nonlinear theory (3.9b).

As h_1 further decreases (or $1/h_1$ increases) (DP_{-1} to DP_{+1}), the WBC increases further as implied by the $\partial_x\psi_B$ term. However, the vorticity balance becomes dramatically different from the weakly nonlinear case. First, dissipation reduces rapidly to become of secondary importance, while the nonlinear advection becomes dominant. Thus, at the lowest order, the vorticity dynamics is inertial;

$$\partial_x\psi_B \sim -[J(\psi_B, \nabla^2\psi_B) + h_eJ(\psi_C, \nabla^2\psi_C)]. \tag{4.4}$$

Second, the barotropic–barotropic interaction becomes stronger than the baroclinic–baroclinic interaction even with a very shallow h_1. Third, the nonlinear advection for both barotropic–barotropic interaction and baroclinic–baroclinic interaction changes sign from that of the weakly nonlinear cases, implying an advection of less anticyclonic relative vorticity northward. This advection is the same sign as in the southern part of Fig. 5b. However, opposite to the southern part, the WBC intensifies. In Fig. 5c for DP_{-1} to DP_{+1}, while the dissipation perturbation remains similar to (4.2), the perturbation planetary vorticity advection is mainly balanced by the perturbation nonlinear advection

streamfunction near the western boundary has already been shifted north (see Fig. 2).

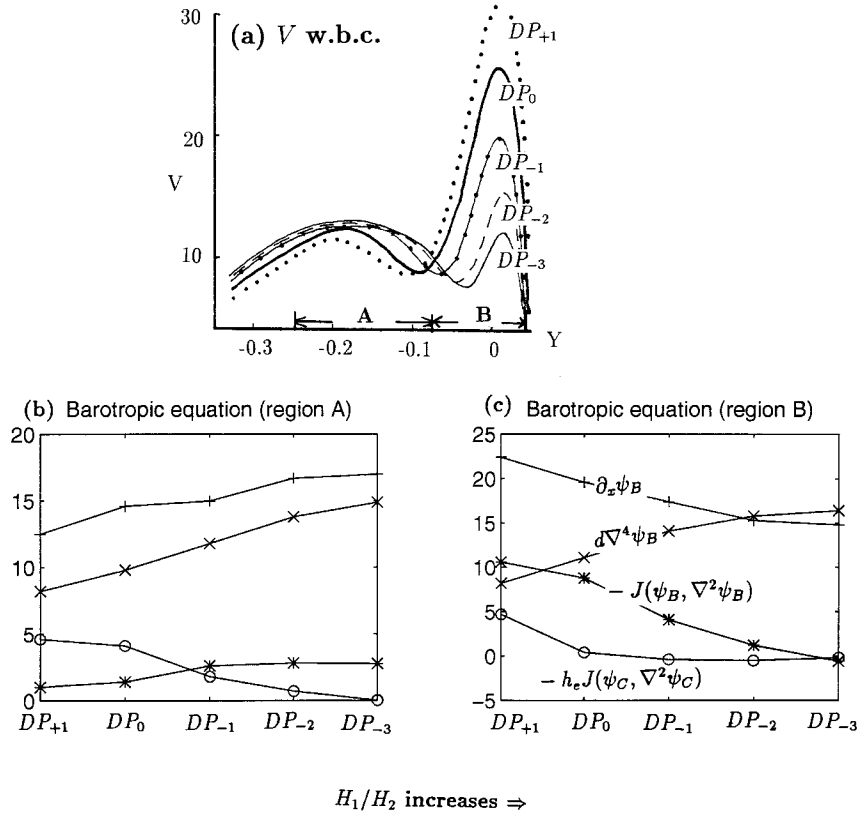

FIG. 5. (a) The meridional variation of the speed of western boundary current (averaged between $x = 0.008$ and $x = 0.031$) for the five DP runs. Term balance for the barotropic equation Eq. (3.1a) is shown for the DP runs in (b) region A and (c) region B, respectively. The local Ekman pumping is always negligible and therefore is not plotted. Region A is located in the middle-south of the subtropical western boundary current, while region B is in the northern part (see Fig. 5a and Fig. 1c). The legend for each term, as indicated in (c), is "+" for $\partial_x\psi_B$, "×" for $d\nabla^4\psi_B$, "−" for w_e, "*" for $-J(\psi_B, \nabla^2\psi_B)$, and "o" for $-h_eJ(\psi_C, \nabla^2\psi_C)$.

$$\frac{\partial(\partial_x\psi_B)}{\partial(1/h_1)} \sim \frac{\partial[-J(\psi_B, \nabla^2\psi_B) + h_eJ(\psi_C, \nabla^2\psi_C)]}{\partial(1/h_1)} > 0. \tag{4.5}$$

In contrast to Eqs. (4.2) and (4.3), the same sign of nonlinear advection term forces the opposite perturbation current in the WBC. As shown at the end of appendix A, this difference is caused by a change of vorticity balance from the dissipation-dominant weakly nonlinear cases to the inertial-dominant strongly nonlinear cases.

In short, the vorticity dynamics in the numerical model supports our theory in the weakly nonlinear cases. The barotropic recirculation can be enhanced significantly by the baroclinic–baroclinic interaction, which intensifies for either a shallower thermocline depth or a stronger reduced gravity. The baroclinic–baroclinic interaction tends to shift the maximum WBC northward and therefore increases the advection of Q anomaly, resulting in enhanced recirculation. Our analyses also show dramatic differences in the vorticity dynamics between a strongly nonlinear case and a weakly nonlinear case, especially in the northern region near the intergyre boundary. Some further discussions on the strongly nonlinear cases will be presented in section 6.

5. Numerical analysis. II: Potential vorticity distribution

We have studied the recirculation in terms of vorticity dynamics. In this section, the recirculation will be studied further, but from the viewpoint of potential vorticity distribution. The Q field in the recirculation has been shown important in determining the penetration of the recirculation. For a given strength of incoming flow, Greatbatch (1988) and MM have shown that the "Fofonoff-like" recirculation ($dq/d\psi > 0$) has a much larger zonal penetration scale than the modonlike recirculation ($dq/d\psi < 0$). In our cases, is it possible for the increased zonal penetration to be caused by a transition from more modonlike to more Fofonoff-like? Before we answer this question, we first have to examine the Q field in order to identify whether our recirculation belongs to

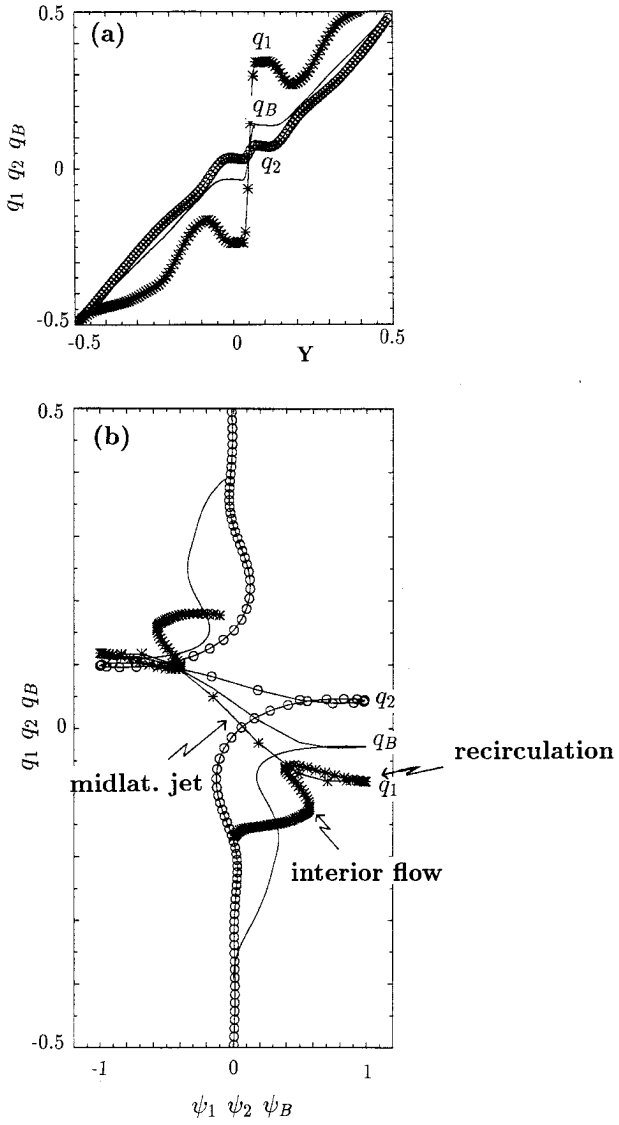

FIG. 6. The potential vorticity profiles for the control run along a longitude section across the core of the recirculation. (a) Potential vorticity for the upper-layer (q_1), the lower-layer (q_2), and the barotropic flow (q_B) as functions of latitude. (b) The same potential vorticity as functions of their corresponding streamfunctions. Each streamfunction is normalized by its maximum value. The corresponding potential vorticity is also rescaled such that the slope $dq/d\psi$ remains unchanged.

modon type or Fofonoff type. Again, we only discuss the DP runs.

a. Q-field in the recirculation

We first examine the Q field in the basin of the control run. In Fig. 6a, we plot Q in the control run along a meridional section across the recirculation core for the upper-layer (q_1), lower-layer, (q_2), and barotropic flows (q_B). Each profile is characterized by three regimes: the midlatitude jet regime, the recirculation regime, and the interior ocean regime. Across the midlatitude jet, q_1 has a sharp gradient, while q_2 has a very weak gradient (the barotropic Q is always the combination of the two). The Q in each layer becomes relatively uniform within the recirculation cell, and is almost identical to the planetary vorticity outside the recirculation. It should be emphasized that the midlatitude jet here refers to those streamlines that will flow beyond the recirculation into the Sverdrup interior. Indeed, the effect of the recirculation, from the vorticity integral point of view, is to produce a strong Q gradient across the midlatitude jet such that the Q anomaly can be dissipated effectively and therefore allow a smooth transition to the interior flow.

The same Q in Fig. 6a is plotted against the streamfunction in Fig. 6b. On each curve, the three regimes of Q that are identified in Fig. 6a can be seen clearly: the midlatitude jet regime, the recirculation regime, and the interior flow regime (in the vicinity of respectively $\psi = 0$ and $q = 0.05$, the maximum and the second maximum of streamfunction). The three regimes are labeled on the q_1 curve. Furthermore, Fig. 6b shows that, on each curve, the slope $dq/d\psi$ is strongly negative in the midlatitude jet regime, only slightly negative (or even uniform) in the recirculation regime, and variable in the interior flow regime. The lower layer is similar to the upper layer except for a much smaller slope $dq_2/d\psi_2$. Thus, we have $dq/d\psi < 0$ in both layers of our recirculation. Furthermore, additional analyses of both the Q field and the vorticity equations show that, except in the western region, Q is almost conserved in the region of recirculation.

b. Modonlike or Fofonoff-like recirculation?

In a baroclinic flow, the proper way to judge the Fofonoff-like or modonlike recirculation is to use the so-called pseudobarotropic mode ψ_A, and the corresponding absolute vorticity q_A (see definition in MM); $dq_A/d\psi_A \geq 0$ favors a resonant Fofonoff mode with a great eastward penetration, while a $dq_A/d\psi_A < 0$ only generates a tight recirculation modonlike mode. Similar to MM, the pseudomodes can be derived straightforward for our general two-layer Q in (2.1c,d) and for the linear relation

$$q_1 = \gamma_1\psi_1 - c_1,\ q_2 = \gamma_2\psi_2 - c_2. \qquad (5.1)$$

One can show that if $\gamma_2 = 0$, the condition for the existence of penetrating mode ($dq_A/d\psi_A \geq 0$) is $\gamma_1 \geq 0$.[2] In Fig. 6, we have seen that in the control run, $dq_2/d\psi_2 = \gamma_2$ is almost zero, and $dq_1/d\psi_1 = \gamma_1$ is slightly negative. Thus, $dq_A/d\psi_A \geq 0$ is not satisfied for the recirculation. In other words, the recirculation in our control run is the modonlike recirculation mode, according

[2] In the notation of (2.1c,d) and (5.1), the necessary and sufficient condition for $dq_A/d\psi_A \geq 0$ is $a(f_1 + f_2) + \gamma_1 + \gamma_2 \geq 0$ and $(af_1 + \gamma_1)(af_2 + \gamma_2) \geq (af_1)(af_2)$.

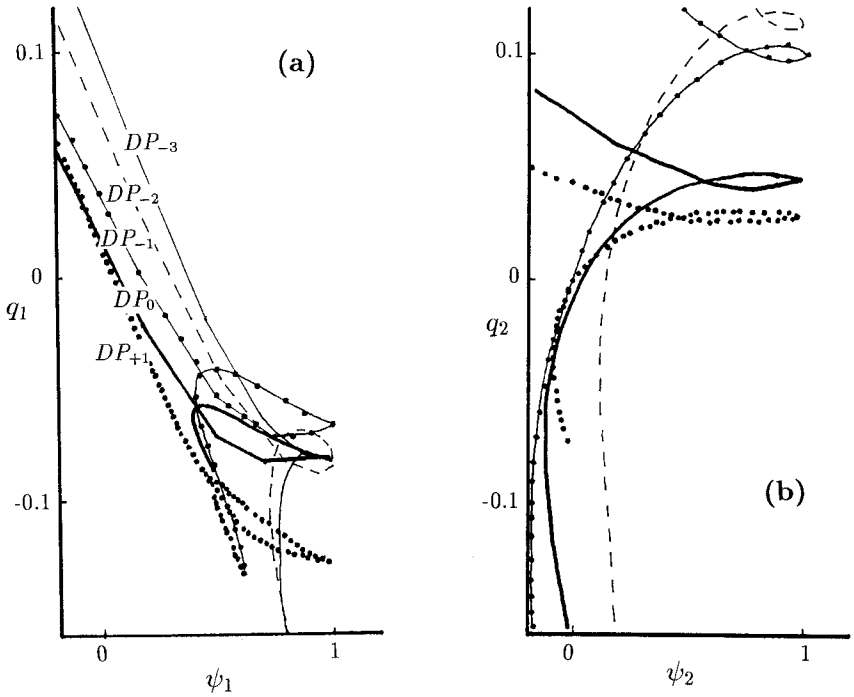

FIG. 7. Upper (a) and lower (b) layer potential vorticity as a function of the streamfunction along a meridional section across the core of the recirculation in each of the five DP runs. Each streamfunction is normalized by its maximum value. The corresponding potential vorticity is also rescaled such that the slope $dq/d\psi$ remains unchanged. Only the part near the recirculation is drawn. In (b), the DP_{-3} case is not drawn because the lower layer has a zero thickness now.

to the definition of MM. This conclusion seems to be independent of the model resolution. because a doubled resolution shows no qualitative difference (not shown).

This modonlike recirculation is also true in other experiments. Figure 7 plots the $q_1(\psi_1)$ and $q_2(\psi_2)$ similar to Fig. 6b, but for the five runs with different thermocline depth. The scales for $q_{1,2}$ have been amplified to show the detailed structure in the recirculation cell. Because the exact Q conservation is not valid, the exact slopes of $dq_1/d\psi_1$ and $dq_2/d\psi_2$ are not definite. Nevertheless, it seems reasonable to use the ''average'' slope within the recirculation cell to represent the $dq_1/d\psi_1$ and $dq_2/d\psi_2$. Visual observation then suggests that the slopes $dq_1/d\psi_1$ and $dq_2/d\psi_2$ are similar to the control run, which is characterized by a slightly negative $dq_1/d\psi_1$ and a virtually zero $dq_2/d\psi_2$. Thus, all our recirculations are modonlike. As a result, the increased penetration for a different thermocline is not due to the transition from a more modonlike recirculation to a more Fofonoff-like recirculation. Then, what causes the intensification of the recirculation?

c. The cause of the greater penetration

For the modonlike recirculation, the penetration scale is inversely proportional to the (square root of) slope $|dq_A/d\psi_A|$, for a given incoming transport (MM). However, the dramatic intensification of recirculation, including its penetration scale (Fig. 2 or Fig. 4a) is not accompanied by an apparent increase of $|dq_A/d\psi_A|$. Indeed, Fig. 7 shows that, while $dq_2/d\psi_2$ remains nearly zero, the slope of $dq_1/d\psi_1$ even decreases slightly. This may seem to contradict the scaling of MM, but it does not. This is because the transports of the incoming flow into the recirculation are different for different runs. Thus, the increased recirculation is forced by the increase in the external (to the recirculation cell) forcing: the western boundary current and its advection of Q anomaly (also see discussion regarding Fig. 4b).

In short, our Q analyses suggest that the recirculation cells in our experiments are modonlike recirculation mode. The intensification is not caused by the transition to a more Fofonoff-like recirculation. Furthermore, the intensification is not controlled by the internal modonlike recirculation itself either. Instead, the intensification is controlled externally by the advection of Q anomaly. This implies that the interaction of the recirculation with the basin-scale ocean gyre is crucial in the intensification of the recirculation.

6. Summary and further discussion

Our two-layer QG model shows that the inertial recirculation is sensitive to the stratification structure. The inertial recirculation can be intensified dramatically by a stratification that favors a stronger upper-layer flow

(or baroclinic flow), such as a shallower thermocline depth or a stronger stratification in the thermocline. A weakly nonlinear theory is presented to explain the mechanism for this intensification. In spite of its limitation, the weakly nonlinear theory does show clearly how the stratification affects the baroclinic–baroclinic interaction, and then feeds back on the barotropic flow of the WBC to enhance the advection of Q anomaly toward the midlatitude jet. The increased Q anomaly is shown to be responsible for the intensification of the recirculation.

From another point of view, the Q-field analyses suggest that our recirculation are modonlike recirculations, rather than the Fofonoff-like penetrating recirculation. The increased zonal penetration scale is caused by the increased advection of the Q anomaly—a forcing external to the recirculation cells, rather than by the transition from a more modonlike solution to a more Fofonoff-like solution, or by the internal dynamics of the modonlike recirculation itself.

One implication of our results is that the barotropic recirculation can be strongly affected by diabatic forcings. This diabatic forcing can be either the local buoyancy forcing (Cushman-Roisin 1987; Huang 1990) or the basinwide entrainment due to the thermohaline circulation. The latter has been confirmed in our preliminary studies. It is found that a basinwide entrainment upwelling can produce a baroclinic flow field that feeds back nonlinearly on the barotropic circulation. The resulted recirculation cell in the subtropical gyre expands toward the subpolar gyre, but with a reduced transport. The opposite occurs for the subpolar gyre.

Although our weakly nonlinear theory is useful for understanding the physical mechanism, it fails to explain some important features in the strongly nonlinear cases, especially in the northern part of the WBC. So far, we have been unable to form a strongly nonlinear theory. Nevertheless, we feel it useful to end the article with comments on some strongly nonlinear features of the recirculation.

First, the analysis at the end of appendix A shows that the advection of relative vorticity has the opposite effect between the strongly nonlinear and weakly nonlinear cases. In the former (latter) case, the nonlinear advection accelerates (decelerates) the southern part but decelerates (accelerates) the northern part of the WBC. Therefore, it is conceivable that something fundamental to the recirculation can change from the weakly nonlinear to the strongly nonlinear case.

Second, three questions regarding Fig. 5c are noteworthy.

(i) Why does the nonlinear advection change its sign from the weakly nonlinear case? For the strongly nonlinear case, a strong recirculation cell appears at the northern end of the WBC. This double-center structure of relative vorticity along the WBC can be inferred from streamfunctions in Fig. 2 or WBC speed in Fig. 5a. Therefore, the WBC still advects less anticyclonic relative vorticity northward in the region south of the recirculation maximum. This region occupies most of the region B in Fig. 5c.

(i) Why is dissipation reduced so rapidly even if the current amplitude is increased? This is caused by the widening of the WBC. Indeed, with the appearance of the recirculation, the zonal width of the WBC increases rapidly and becomes comparable to or even larger than the meridional scale. This creates a dramatic reduction of dissipation, which is inversely proportional to the Fourth power of the boundary layer width.

(ii) Why does the barotropic–barotropic interaction remain strong even with a small h_1? This seems to be related to the nature of the recirculation, which is dominated by a barotropic core. An intensified recirculation is usually accompanied by a stronger barotropic current and in turn the barotropic relative vorticity advection. Thus, in Fig. 5c, while the baroclinic vorticity advection increases when h_1 decreases, the barotropic vorticity advection also increases.

Furthermore, special attention should be paid to the dynamic linkage between the recirculation and the western boundary current. As shown in both the vorticity dynamics and the Q-field analysis, the strength of the recirculation is determined critically by the strength of the advection of Q anomaly. This Q anomaly cannot be determined in regional models, such as those of C88 and MM. C88 shows that for a given Q anomaly the barotropic transport of the recirculation decreases with the intensity of the stratification.[3] This is the opposite to our results if we do not take into account the variation of the Q-anomaly forcing. It seems likely that a strongly nonlinear theory should include the dynamic linkage between the WBC and the recirculation, which is crucial in determining the Q anomaly. This poses a challenging problem.

Finally, if we accept the concept of Greatbatch (1988) and MM, the modonlike solution may differ significantly between ours and theirs. Their prototype modon type has a motionless background flow field. In our case, the background flow is strong, especially along the midlatitude jet and the western boundary. It is likely that the strong source of Q can change the dynamics of the free modon significantly to some type of boundary-forced modon.

Acknowledgments. The author thanks Dr. J. Pedlosky for discussions on the perturbation solution in appendix A. The comments from Dr. G. Nurser and an anonymous reviewer have improved the manuscript greatly. This work is supported by NSF and the Young Investigator Award of ONR.

[3] In C88's notation, an increased reduced gravity leads to the decrease of the parameter α_1. Her Fig. 5 then shows the lower-layer recirculation width l_2 will decrease. Then, her Eq. (4.5) shows that the barotropic transport decreases.

APPENDIX A

Barotropic–Barotropic Interaction on Barotropic Flow

We only discuss the free-slip boundary condition case since the no-slip case is similar. In order to avoid secular terms, we define a slow boundary layer variable $s = \epsilon\xi$ (J. Pedlosky 1993, personal communication). Then, we use the following multiple scale method to expand Eq. (3.3a) in the absence of ψ_C. Using the expansion in (3.8) and $\partial_\xi = \partial_\xi + \epsilon\partial_s$ at the lowest order, Eq. (3.3a) becomes

$$(-\partial_{\xi\xi\xi} + 1)\partial_\xi\psi_{B0} = 0. \tag{A.1}$$

With the boundary conditions

$$\psi_{B0}\,|_{\xi=0} = 0,\ \partial_{\xi\xi}\psi_{B0}\,|_{\xi=0} = 0,\ \psi_{B0}\,|_{\xi\to\infty} = \psi_{BI}(0,y), \tag{A.2}$$

we have the solution

$$\psi_{B0} = \psi_{BI}(x, y) - A(s, y)p(\xi), \tag{A.3}$$

where

$$p(\xi) = \left[\cos\left(\frac{\sqrt{3}}{2}\xi\right) - \frac{1}{\sqrt{3}}\sin\left(\frac{\sqrt{3}}{2}\xi\right)\right]e^{-\xi/2}.$$

The amplitude A will be determined at the next order with the boundary condition

$$A(0, y) = \psi_{BI}(0, y). \tag{A.4}$$

At the next order, using the first-order solution above, we have the equation

$$\begin{aligned}(-\partial_{\xi\xi\xi} + 1)\partial_\xi\psi_{B1} &= -J(\psi_{B0}, \nabla^2\psi_{B0})\\ &= -(3\partial_s A - u_{BI}A)p(\xi) + A\partial_y A e^{-\xi},\end{aligned} \tag{A.5}$$

where $u_{BI} = -\partial_y\psi_{BI}$. The conditions for the removal of secular terms give $3\partial_s A - u_{BI}A = 0$. With the boundary condition (A.4), we have $A = \psi_{BI}(0, y)\exp(u_{BI}s/3)$. One can verify that the boundary layer width is modified to $\delta = \delta_M/[1 - 3(\delta_I/\delta_M)^2 u_{BI}(y)]$. The boundary layer width is wider than the linear model in the northern part of the subtropical gyre, but narrower in the southern part. (This modification to the width is opposite to Stommel's boundary layer case!)

Now, we solve the second-order barotropic solution forced by the nonsecular terms on the rhs of (A.5). The solution that satisfies the boundary conditions

$$\begin{aligned}&\psi_{B1}(\xi = 0) = 0,\\ &\partial_{\xi\xi}\psi_{B1}(\xi = 0) = -2\partial_s A\frac{dp}{d\xi}(\xi = 0, s = 0),\end{aligned} \tag{A.6}$$

and the interior matching condition is

$$\psi_{B1} = \frac{\partial_y A^2}{4}\left\{e^{-\xi/2}\left[\cos\left(\frac{\sqrt{3}}{2}\xi\right) - 17\sqrt{3}\sin\left(\frac{\sqrt{3}}{2}\xi\right)/9\right] - e^{-\xi}\right\}. \tag{A.7}$$

At the western boundary $\xi = s = 0$, notice (A.4), we have

$$v_{B1}|_{\xi=0} = [-p\partial_s A + \partial_{B1\xi}\psi]\,|_{\xi=0,s=0} = -5\partial_y(\psi_{BI}^2)/12. \tag{A.8}$$

For a subtropical gyre, this means that the WBC is decelerated (accelerated) in the south (north) of the maximum interior streamfunction. In other words, the maximum WBC is shifted toward the intergyre boundary.

Physically, the variation of the WBC intensity with the nonlinear advection term can be understood in the following. In the southern (northern) part of the WBC, less (more) anticyclonic relative vorticity is advected northward, that is, $-J(\psi_B, \nabla^2\psi_B) > 0$ ($-J(\psi_B, \nabla^2\psi_B) < 0$). This tends to reduce (enhance) the local anticyclonic vorticity and therefore reduces (enhances) the diffusion of anticyclonic vorticity toward the interior. Thus, at lowest order, the linear vorticity balance (A.1) requires weaker (stronger) planetary vorticity advection, implying a weaker (stronger) boundary current.

The above discussion is under the assumption of weak nonlinearity. Is the conclusion still valid when nonlinearity becomes dominant? With the inertial balance

$$\partial_x\psi_B \sim -J(\psi_B, \nabla n^2\psi_B), \tag{A.9}$$

we find that $v_B = \partial_x\psi_B \sim -J(\psi_B, \nabla^2\psi_B) > 0$, south of the maximum relative vorticity, and $v_B = \partial_x\psi_B \sim -J(\psi_B, \nabla^2\psi_B) < 0$ north of the maximum relative vorticity. Thus, the effect of nonlinear advection of relative vorticity is to accelerate (decelerate) the WBC in the southern (northern) part. Physically, in the southern (northern) part where the relative vorticity becomes more negative (decreases) toward the north, Q conservation requires an increase (decrease) of planetary vorticity, implying a northward (southward) current. This analysis agrees with the numerical experiments in the northern part of the western boundary current as shown in Eqs. (4.4) and (4.5).[4] Thus, the nonlinear advection effect on the WBC speed is exactly the opposite between the strongly nonlinear case and the weakly nonlinear case in (A.8)!

This difference is caused by the fact that the nonlinearity is mainly balanced by the diffusion in the weakly nonlinear case. Indeed, with the solution in (A.7), one can easily show that at the western boundary, $-\partial_{\xi\xi\xi\xi}\psi_{B1}\,|_{\xi=0} = 3\partial_\xi\psi_{BI}^2/4$, $\partial_\xi\psi_{B1}\,|_{\xi=0} = -\partial_\xi\psi_{BI}^2/4$. On the other hand, after the removal of secular terms, the nonlinear interaction term is $-J(\psi_{B0}, \partial_{\xi\xi}\psi_{B0})\,|_{\xi=0} = \partial_\xi\psi_{BI}^2/2$. The full vorticity balance at the western boundary is then

$$-\partial_{\xi\xi\xi\xi}\psi_{B1} + \partial_\xi\psi_{B1} = -J(\psi_{B0}, \partial_{\xi\xi}\psi_{B0}) \text{ at } \xi = 0.$$

Notice that the planetary advection term has the opposite

[4] Here we have not considered the matching with the interior flow. Only the northward WBC in the southern part can match the interior flow and therefore is physically plausible (e.g., Pedlosky 1987).

sign to the local nonlinear advection. The dominant balance for the nonlinear term is the lateral dissipation term

$$-\partial_{\xi\xi\xi\xi}\psi_{B1} \sim -J(\psi_{B0}, \partial_{\xi\xi}\psi_{B0}). \quad \text{(A.10)}$$

The speed of the WBC is then determined by the Munk-type dissipation balance between the advection of planetary vorticity and lateral mixing as

$$\partial_\xi\psi_{B1} \sim \partial_{\xi\xi\xi\xi}\psi_{B1} - J(\psi_{B0}, \partial_{\xi\xi}\psi_{B0}) \sim \partial_{\xi\xi\xi\xi}\psi_{B1}. \quad \text{(A.11)}$$

This analysis agrees with the numerical experiments in the southern part of the western boundary current as shown in Eqs. (4.1), (4.2), and (4.3).

APPENDIX B

Baroclinic–Baroclinic Interaction on Barotropic Flow

At lowest order, Eqs. (3.3a,b) give the Munk layer problem

$$[-\partial_{\xi\xi\xi} + 1]\partial_\xi\psi_{B0} = 0 \quad \text{(B.1a)}$$

$$[-(\partial_{\xi\xi} - b)\partial_\xi + 1]\partial_\xi\psi_{C0} = 0. \quad \text{(B.1b)}$$

The boundary conditions are (A.3) and

$$\psi_{C0}\,|_{\xi=0} = 0,\ \partial_{\xi\xi}\psi_{C0}\,|_{\xi=0} = 0,\ \psi_{C0}\,|_{\xi\to\infty} = \psi_{CI}(0, y). \quad \text{(B.2)}$$

The barotropic solution is the same as (A.3). To derive the baroclinic solution, we substitute $\psi_{C0} \sim \exp(\lambda\xi)$ into (B.1b) to derive the eigenvalue equation: $\lambda^3 - b\lambda = 1$. One root is real and positive. The other two roots have negative real parts. They are real or complex depending on whether b exceeds the critical value $b_c = 3 \times 2^{-2/3}$;

$$\lambda = -\gamma + i\mu,\ -\gamma - i\mu \quad \text{for} \quad b_c > b > 0,$$
$$\lambda = -\gamma_1,\ -\gamma_2, \quad \text{for} \quad b \geq b_c. \quad \text{(B.3)}$$

Here we have chosen $\gamma \geq 0$, $\mu \geq 0$, and $\gamma_1 \geq \gamma_2 \geq 0$. These eigenvalues are plotted in Fig. B1b. The baroclinic solution therefore is

$$\psi_{C0} = \psi_{CI}\left\{1 - e^{-\gamma\xi}\left[\cos(\mu\xi) + \frac{\gamma^2 - \mu^2}{2\gamma\mu}\sin(\mu\xi)\right]\right\} \quad \text{for } b_c > b > 0 \quad \text{(B.4a)}$$

$$\psi_{C0} = \psi_{CI}\left[1 + \frac{1}{\gamma_1^2 - \gamma_2^2}(\gamma_2^2 e^{-\gamma_1\xi} - \gamma_1^2 e^{-\gamma_2\xi})\right] \quad \text{for } b > b_c. \quad \text{(B.4b)}$$

At the next order, the barotropic equation can be derived from (3.3a) as

$$[-\partial_{\xi\xi\xi} + 1]\partial_\xi\psi_{B1} = -J(\psi_{B0},\partial_{\xi\xi}\psi_{B0}) - h_e J(\psi_{C0},\partial_{\xi\xi}\psi_{C0}). \quad \text{(B.5)}$$

The solution due to the first term has been discussed in appendix A [see Eq. (A.7)]. For the part forced by the second term, we substitute (B.4) into (B.5). With the boundary condition

$$\psi_{C1}(\xi = 0) = 0,\ \partial_{\xi\xi}\psi_{C1}(\xi = 0) = 0,$$

the solution can be derived:

$$\psi_{B1}^C = -h_e\partial_y(\psi_{CI}^2)F_1\left\{a_0 e^{-2\gamma\xi} + e^{-\gamma\xi}[a_1\cos(\mu\xi) + a_2\sin(\mu\xi)] + e^{-\xi/2}\left[b_1\cos\left(\frac{\sqrt{3}}{2}\xi\right) + b_2\sin\left(\frac{\sqrt{3}}{2}\xi\right)\right]\right\}$$
for $b_c > b > 0$ (B.6a)

$$\psi_{B1}^C = h_e\partial_y(\psi_{CI}^2)F_2\left\{c_0 e^{-(\gamma_1+\gamma_2)\xi} + c_1 e^{-\gamma_1\xi} + c_2 e^{-\gamma_2\xi} + e^{-\xi/2}\left[d_1\cos\left(\frac{\sqrt{3}}{2}\xi\right) + d_2\sin\left(\frac{\sqrt{3}}{2}\xi\right)\right]\right\}$$
for $b > b_c$. (B.6b)

Here the coefficients are

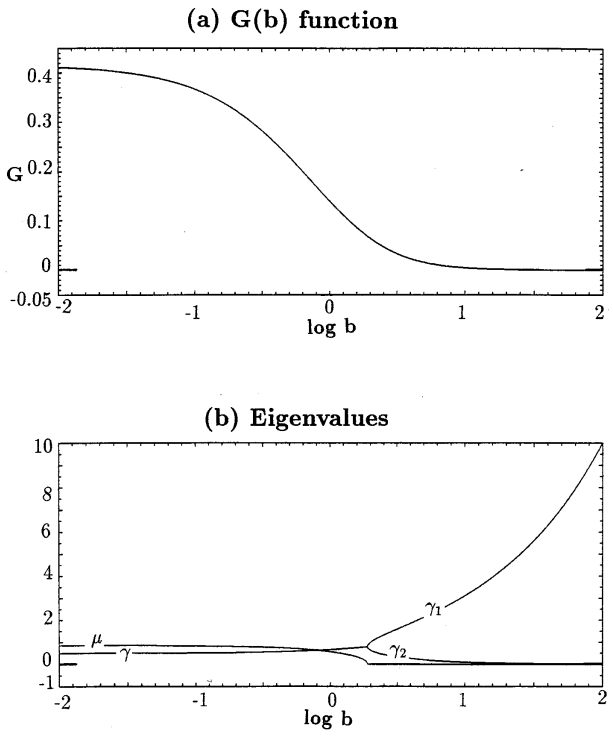

FIG. B1. (a) The function $G(b)$ as defined in Eq. (B.8) as a function of the stratification parameter b. (b) The eigenvalues for the Munk problem of the baroclinic mode [see (B.3) for definitions of the curves.]

$$F_1 = (\gamma^2 + \mu^2)^2/4\gamma\mu,\ a_0 = \mu/2\gamma(1 + 8\gamma^3),$$

$$a_1 = \mu(3\gamma^2 - \mu^2)/N,\ a_2 = [1 - \gamma(3\mu^2 - \gamma^2)]/N,$$

$$N = [1 - \gamma(3\mu^2 - \gamma^2)]^2 + \mu^2(3\gamma^2 - \mu^2)^2,$$

$$b_1 = -(a_0 + a_1),$$

$$b_2 = \{8\gamma^2 a_0 - 2[(\mu^2 - \gamma^2)a_1 + 2\gamma\mu a_2] - b_1\}/\sqrt{3},$$

$$F_2 = \gamma_1^2\gamma_2^2/2(\gamma_1^2 - \gamma_2^2),$$

$$c_0 = -(\gamma_1 - \gamma_2)/(\gamma_1 + \gamma_2)[1 + (\gamma_1 + \gamma_2)^3],$$

$$c_1 = 1/(1 + \gamma_1^3),\ c_2 = -1/(1 + \gamma_2^3),$$

$$d_1 = -(c_0 + c_1 + c_2),$$

$$d_2 = 2[(\gamma_1 + \gamma_2)^2 c_0 + \gamma_1^2 c_1 + \gamma_2^2 c_2 - d_1/2]/\sqrt{3}.$$

The meridional velocity on the western boundary can be derived as

$$v_{B1}^C(\xi = 0) = \partial_\xi \psi_{B1}^C(\xi = 0) = -h_e \partial_y(\psi_{CI}^2)G. \quad \text{(B.7)}$$

Here G is a function of the eigenvalues, which are functions of b, thus $G = G(b)$. It is defined as

$$G = F_1\left\{4a_0\left[\left(\gamma - \frac{1}{4}\right)^2 + \frac{3}{16}\right] + a_1\left[\left(\gamma - \frac{1}{2}\right)^2 + \frac{3}{4} - \mu\right] + 2\mu a_2\left(\frac{1}{2} - \gamma\right)\right\} \quad \text{for } b_c > b > 0 \quad \text{(B.8a)}$$

$$G = \frac{\gamma_1^2\gamma_2^2}{2(\gamma_1 + \gamma_2)}\left[\frac{1}{(\gamma_1 + \gamma_2)(1 + \gamma_1 + \gamma_2)} + \frac{1}{(1 + \gamma_1)(1 + \gamma_2)}\right] \quad \text{for } b \geq b_c. \quad \text{(B.8b)}$$

The function G is plotted in Fig. B1a. It starts from a positive value (about 0.45) at $b = 0$ and decreases monotonically to zero at $b \to \infty$.

REFERENCES

Bryan, K., 1963: A numerical investigation of a nonlinear model of a wind-driven ocean. *J. Atmos. Sci.*, **20,** 594–606.

Cessi, P., 1988: A stratified model of the inertial recirculation. *J. Phys. Oceanogr.*, **18,** 662–682.

——, G. Ierley, and W. R. Young, 1987: A model of the inertial recirculation driven by potential vorticity anomalies. *J. Phys. Oceanogr.*, **17,** 1640–1652.

Cushman-Roisin, B., 1987: On the role of heat flux in the Gulf Stream–Sargasso Sea subtropical gyre system. *J. Phys. Oceanogr.*, **17,** 2189–2202.

Greatbatch, R. J., 1987: A model for the inertial recirculation of a gyre. *J. Mar. Res.*, **45,** 601–634.

——, 1988: On the scaling of inertial subgyres. *Dyn. Atmos. Oceans*, **12,** 265–285.

Hogg, N. G., 1983: A note on the deep circulation of the western North Atlantic Ocean. *Deep-Sea Res.*, **30,** 945–961.

Holland, W., and P. Rhines, 1980: An example of eddy-induced ocean circulation. *J. Phys. Oceanogr.*, **10,** 1010–1031.

Huang, R. X., 1990: Does atmospheric cooling drive the Gulf Stream recirculation? *J. Phys. Oceanogr.*, **20,** 750–757.

Ierley, G., 1987: On the onset of inertial recirculation in a barotropic general circulation model. *J. Phys. Oceanogr.*, **17,** 2366–2374.

——, and W. R. Young, 1988: Inertial recirculation in a β-plane corner. *J. Phys. Oceanogr.*, **18,** 683–689.

Marshall, D., and J. Marshall, 1992: Zonal penetration scale of mid-latitude oceanic jets. *J. Phys. Oceanogr.*, **22,** 1018–1032.

Marshall, J., and A. Nurser, 1986: Steady, free circulation in a stratified quasigeostrophic ocean. *J. Phys. Oceanogr.*, **16,** 1799–1813.

Pedlosky, J., 1987: *Geophysical Fluid Dynamics.* Springer-Verlag, 710 pp.

Richardson, P. L., 1985: Average velocity and transport of the Gulf Stream near 55°W. *J. Mar. Res.*, **43,** 83–111.

Schmitz, W. J., 1980: Weakly-depth-dependent segments of the North Atlantic circulation. *J. Mar. Res.*, **38,** 111–133.

Worthington, L. V., 1976: *On the North Atlantic Circulation.* The Johns Hopkins University Press, 110 pp.

Wunsch, C., and B. Grant, 1982: Towards the general circulation of the North Atlantic Ocean. *Progress in Oceanography*, Vol. 11, Pergamon, 1–59.